.

Accurate global potential energy surface for the H + OH$^+$ collision

M. A. Gannouni, N. E. Jaidane, P. Halvick' , T. Stoecklin, and M. Hochlaf'

Accurate global potential energy surface for the H + OH$^+$ collision

M. A. Gannouni,[1,2] N. E. Jaidane,[1] P. Halvick,[3,a)] T. Stoecklin,[3] and M. Hochlaf[2,a)]
[1]*Laboratoire de Spectroscopie Atomique, Moléculaire et Applications – LSAMA, Université de Tunis El Manar, Tunis, Tunisia*
[2]*Laboratoire Modélisation et Simulation Multi Echelle, Université Paris-Est, MSME UMR 8208 CNRS, 5 bd Descartes, 77454 Marne-la-Vallée, France*
[3]*Institut des Sciences Moléculaires, Université de Bordeaux, CNRS UMR 5255, 33405 Talence Cedex, France*

We mapped the global three-dimensional potential energy surface (3D-PES) of the water cation at the MRCI/aug-cc-pV5Z including the basis set superposition (BSSE) correction. This PES covers the molecular region and the long ranges close to the H + OH$^+$($X^3\Sigma^-$), the O + H$_2^+$($X^2\Sigma_g^+$), and the hydrogen exchange channels. The quality of the PES is checked after comparison to previous experimental and theoretical results of the spectroscopic constants of H$_2$O$^+$($\tilde{X}^2B_1$) and of the diatomic fragments, the vibronic spectrum, the dissociation energy, and the barrier to linearity for H$_2$O$^+$($\tilde{X}^2B_1$). Our data nicely approach those measured and computed previously. The long range parts reproduce quite well the diatomic potentials. In whole, a good agreement is found, which validates our 3D-PES. © *2014 AIP Publishing LLC*. [http://dx.doi.org/10.1063/1.4872329]

I. INTRODUCTION

Up-to-date experimental investigations of bimolecular collisions are of great precision. Their interpretation requires outstanding efforts from theoreticians, who can provide accurate spectroscopic and collisional data directly comparable to experiment.[1–5] At first glance, an accurate global potential energy surface is mandatory. Recently, this was achieved globally for several atmospherically and astrophysically relevant molecular species such as HCO,[6,7] H$_3^+$,[8] H$_2$O,[9] and ozone.[10]

In the present contribution, we generate the global three-dimensional potential energy surface (3D-PES) of doublet spin multiplicity for the H(^{2}S) + OH$^+$($X^3\Sigma^-$) collision. This reactive channel leads, for instance, to the formation of water cation in its ground electronic state, H$_2$O$^+$($\tilde{X}^2B_1$) as can be seen in Figure 1, which presents the energetic diagram of the lowest dissociation limits of the H$_2$O$^+$ cation constructed based on data from Ref. 11.

The production of H$_2$O$^+$ through the collisions between H and OH$^+$ may be relevant for the chemistry of interstellar media and of the upper atmosphere.[12] Indeed, OH$^+$ and H$_2$O$^+$ are among the fundamental building blocks of these media. They were detected in comet tails[13] and in interstellar clouds.[14] In addition, they are used, together with H$_3$O$^+$, as probes of cosmic ray ionization rates.[15] Especially, the reactive processes involving these cations are expected to influence the dependence of ortho-H$_2$O$^+$/para-H$_2$O$^+$ ratio upon the temperature on these media.[16]

In the literature, a substantial body of data exists on the energetics (potential barriers, dissociation energies) and on the spectroscopy of the H$_2$O$^+$ intermediate. Their comparison to those deduced from our 3D-PES represents critical tests for its validation. In related topic, Martínez *et al.*[17]

generated the PES of quartet spin-multiplicity for the formation of H(^{2}S) + OH$^+$($X^3\Sigma^-$) as products of the O$^+$(^{4}S) + H$_2$($X^1\Sigma_g^+$) collision. This PES was incorporated into dynamical nuclear treatments to deduce the cross sections for the O$^+$(^{4}S) + H$_2$($X^1\Sigma_g^+$) $\rightarrow$ H(^{2}S) + OH$^+$($X^3\Sigma^-$) reaction and its isotopic variants,[17–22] where the reaction is constrained to evolve solely on the quartet PES. However, no similar studies were performed on the lowest doublet PES that correlates to the ground state of water cation for elucidation of its role during these ion-molecule reactions.

The H$_2$O$^+$($\tilde{X}^2B_1$) $\rightarrow$ OH$^+$ ($X^3\Sigma^-$) + H(^{2}S) reaction, the sole fragmentation pathway at threshold was widely investigated. Recently, Ashfold and co-workers[23] presented velocity map imaging studies of the photodissociation of H$_2$O$^+$ cation and reviewed both previous experimental and theoretical treatments dealing with this reaction. Moreover, these authors computed the cuts through the PESs for the lowest doublet and quartet states of H$_2$O$^+$. This was done at the MRCI+Q/aug-cc-pVTZ level along the bending coordinate and by lengthening one OH distance updating hence the theoretical works by Lorquet and co-workers.[24,25] Afterwards, two mechanisms were identified: the first one involves Renner-Teller coupling to the ground state PES. The second requires spin-orbit induced conversion to the repulsive $\tilde{a}^4B_1(^4A'')$ state PES, which correlates also adiabatically to the H(^{2}S) + OH$^+$($X^3\Sigma^-$) channel. The first mechanism enlightens the importance of considering the ground state of H$_2$O$^+$ in these bimolecular processes.

The spectroscopy of H$_2$O$^+$($\tilde{X}^2B_1$) is well documented as well. In 1993, Rosmus and co-workers[26] presented a detailed comprehensive theoretical spectroscopic treatment of H$_2$O$^+$($\tilde{X}^2B_1$ and $\tilde{A}^2A_1$) states that form a linear-bent Renner-Teller system with non-zero spin-orbit contribution. They generated the 3D-PESs of both states using MRCI. Then, the spin-rovibronic spectrum was calculated variationally taking into account all couplings including Renner-Teller and

---

a)Authors to whom correspondence should be addressed. Electronic addresses: p.halvick@ism.u-bordeaux1.fr and hochlaf@univ-mlv.fr
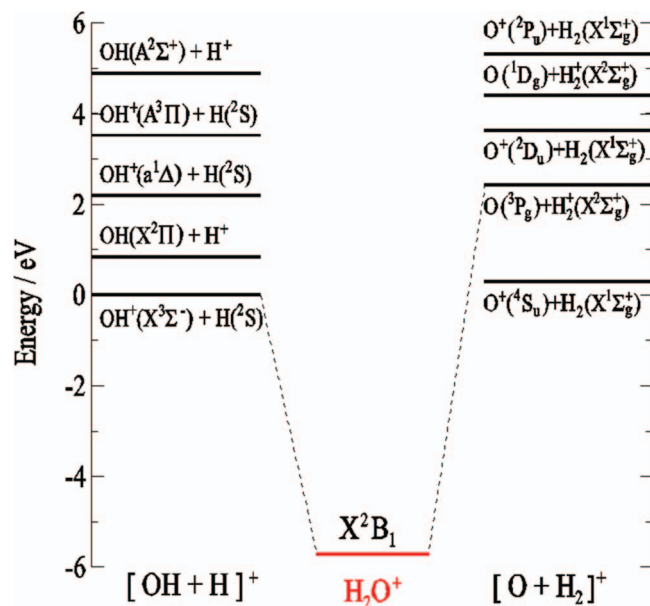
FIG. 1. Energetic diagram of the lowest dissociation limits of the H_2O^+ cation. The energies are given with respect to the $OH^+(X^3\Sigma^-) + H(^2S)$ dissociation limit. The asymptotes are positioned in energy using the data from Ref. 11. The dashed line corresponds to the correlation diagram of $H_2O^+(\tilde{X}^2B_1)$.

spin-orbit effects. Afterwards, several other theoretical treatments were done dealing with the vibronic bands (energy positions and intensities) allowing hence close analysis for the Photoelectron spectrum of water and of the nonadiabatic effects undergone by H_2O^+ lowest electronic state.[27,28] Various experimental investigations validated these findings and at-

TABLE I. Numerical values of the parameters (c_j) in Eq. (7).

c_j	Value	c_j	Value
c_0	0.357287	c_{25}	− 0.026406
c_1	− 0.011409	c_{26}	− 0.080664
c_2	0.118401	c_{27}	0.136792
c_3	0.636078	c_{28}	0.043168
c_4	0.598602	c_{29}	− 0.011388
c_5	− 1.466868	c_{30}	− 0.087928
c_6	0.325729	c_{31}	0.126219
c_7	− 0.511031	c_{32}	0.039293
c_8	− 0.998473	c_{33}	0.046195
c_9	0.108664	c_{34}	0.005922
c_{10}	1.330627	c_{35}	0.003550
c_{11}	0.140430	c_{36}	0.013295
c_{12}	0.189295	c_{37}	− 0.000008
c_{13}	0.240802	c_{38}	0.030656
c_{14}	0.481531	c_{39}	0.056742
c_{15}	0.369386	c_{40}	0.003726
c_{16}	0.109044	c_{41}	− 0.014745
c_{17}	− 0.618908	c_{42}	− 0.006200
c_{18}	− 0.142950	c_{43}	0.009663
c_{19}	− 0.077827	c_{44}	0.005874
c_{20}	0.143510	c_{45}	− 0.002847
c_{21}	− 0.159928	c_{46}	− 0.008690
c_{22}	− 0.056145	c_{47}	− 0.013496
c_{23}	− 0.059548	c_{48}	0.032732
c_{24}	− 0.253655	c_{49}	− 0.028818

tested on the high quality of the predictions of Rosmus and co-workers.[29–40]

As stated above, the full understanding of the title reaction mechanism is of great importance to determine the relative abundances of OH^+ and H_2O^+ for better modeling of the ionic chemistry of the atmosphere and of the Interstellar medium (ISM). This goes through the generation of an accurate global 3D-PES for the $H + OH^+ \leftrightarrow H_2O^+$ reactive process. Nevertheless, previous works were limited either to one dimensional cuts through the PESs for the lowest doublet and quartet states of H_2O^+ or to the generation of 3D-PES of H_2O^+ for spectroscopic purposes and hence not close enough to the dissociation channels. The 3D-PES of Martínez *et al.*[17] is of quartet spin-multiplicity, whereas one needs a doublet potential to account for the title reaction. Here, we remediate towards this deficiency. Indeed, we mapped the 3D-PES of doublet spin multiplicity. This was done at the MRCI level in connection with a large basis set. Then, we deduced an analytical representation of this PES, which was incorporated into nuclear motion treatment to calculate the rovibronic spectrum of $H_2O^+(\tilde{X}^2B_1)$. The energetics (such as the potential barriers, dissociation energies), and the asymptotic behavior of this analytical form of our PES are also compared to the available experimental data. In whole, a good agreement is found validating, hence, our global 3D-PES.

II. GENERATION OF THE 3D PES

All electronic calculations were performed using the MOLPRO program suite, in the C_s point group.[41] Because of the multiconfigurational nature of the electronic wavefunction of $H_2O^+(\tilde{X}^2B_1)$, these calculations were done using the Complete Active Space Self Consistent Field (CASSCF)[42,43] method followed by the internally contracted Multi Reference Configuration Interaction (MRCI)[44,45] approach in connection with the aug-cc-pV5Z basis set of Dunning and co-workers.[46–49] In the CASSCF active space, all valence molecular orbitals were optimized, which include the $2s$, $2p$ atomic orbitals for O and $1s$ for H. The core orbital ($1s$ of O) was frozen at the CASSCF level of theory. In MRCI, all configurations of the CASSCF wavefunctions were taken into account as reference.

The 3D-PES of $H_2O^+(\tilde{X}^2B_1)$ was mapped in Jacobi coordinates (R_2, ρ_2, φ_2) (Figure 2). The center of coordinates is placed in the center of mass of the OH fragment and the vector ρ_2 connects this center and the second hydrogen. The calculations were performed for several OH distances (R_2 = 1.3, 1.5, 1.6, 1.7, 1.837, 1.9, 1.91, 1.92, 1.93, 1.94, 2.0, 2.5, 3.0, 4.0, 5.0; in bohr). For each R_2, φ_2 varies from 0° to 180° by step of 5° and ρ_2 takes values distribute in the [1, 50] interval. The grid on ρ_2 is not regular: the step was of 0.1 for $\rho_2 \in [1, 2.9]$, of 0.25 for $\rho_2 \in [3, 15]$, of 1 for $\rho_2 \in [16, 25]$, and of 10 for $\rho_2 \in [30, 50]$ (all values are in bohr). In total, 25 515 non-equivalent total energies were computed.

In all calculations, to determine the interaction potential, V, the basis set superposition error (BSSE) was corrected at all geometries with the Boys and Bernardi counterpoise
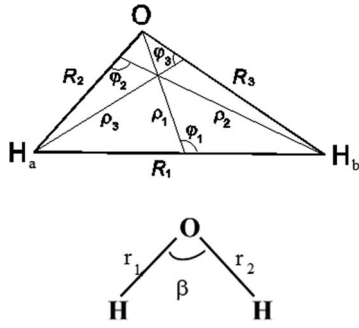
FIG. 2. Definition of the coordinate system used for the generation of the 3D-PES. Upper panel: R_1, R_2, and R_3 are the internuclear distances of Eq. (2). Lower panel: r_1, r_2, and β are the internal coordinates used in Eq. (16).

scheme[50]

$$V = E(H_2O^+) - E(OH^+) - E(H), \qquad (1)$$

where the energies of the OH^+ and H subsystems are computed in a full basis set of the complex. At equilibrium, the BSSE accounts for 0.09% of the interaction energy. At large internuclear distances ($\rho_2 = 8$ bohrs), the BSSE amounts to 0.1%.

III. ANALYTIC FORM

The global doublet potential energy surface for the H_2O^+ system should cover the global minimum along with the dissociation channels $H(^2S) + OH^+(X^3\Sigma^-)$, $O(^3P) + H_2^+(X^2\Sigma_g^+)$. Let us note that the two $H + OH^+$ channels will be differentiated by denoting them as $H_a + OH_b^+$ and $H_b + OH_a^+$ when necessary. The functional form is based on the many-body expansion. It is written as the sum of two-body $V^{(2)}$ and three-body $V^{(3)}$ terms

$$V(R_1, R_2, R_3) = V^{(2)}_{H_aH_b}(R_1) + V^{(2)}_{OH_a}(R_2) + V^{(2)}_{OH_b}(R_3)$$
$$+ V^{(3)}(R_1, R_2, R_3), \qquad (2)$$

where R_1, R_2, and R_3 are the internuclear distances as defined in Figure 2.

The two-body potentials have been built within the framework of the Reproducing Kernel Hilbert Spaces (RKHS) method.[51,52] In the case of 1D semi-infinite interval $[0,\infty]$, the reciprocal power reproducing kernel $q^{n,m}$ is convenient because its long-range behavior scales[53] as R^{-m-1} and R^{-m-2}. The main interaction, occurring in the vicinity of the dissociations forming the OH^+ or H_2^+ diatomic molecules, is a charge-induced dipole interaction.[54] Thus, the value $m = 3$ is used.

With N data points x_j, the RKHS interpolated energy curve for any diatomic molecule can be written

$$V^{(2)}(R) = \sum_{j=1}^{N} c_j q^{2,m}(R, x_j). \qquad (3)$$

For $n = 2$, the kernel $q^{n,m}$ is given by

$$q^{2,m}(x, x') = \frac{4x_>^{-m-1}}{(m+1)(m+2)}\left(1 - \frac{(m+1)x_<}{(m+3)x_>}\right),$$
$$x_> = \max(x, x'), \qquad (4)$$
$$x_< = \min(x, x').$$

The three-body potential $V^{(3)}$ is the sum of two terms V_{SR} and V_{LR} that represent the short-range part and the long-range part of the potential energy, respectively.

$$V^{(3)}(R_1, R_2, R_3) = V_{SR}(R_1, R_2, R_3) + V_{LR}(R_1, R_2, R_3). \qquad (5)$$

V_{SR} is defined as a product of a 3D polynomial and a damping function[55,56]

$$V_{SR}(R_1, R_2, R_3) = P(Q_1, Q_2, Q_3)$$
$$\times \prod_{i=1}^{3}[(1 - \tanh(\gamma_i(R_i - R_i^0))/2)], \qquad (6)$$

where $\gamma_1 = 0.35$; $\gamma_2 = 0.6$; $\gamma_3 = 0.6$, $R^0_1 = 1.2$, $R^0_2 = 2.6$, $R^0_3 = 2.6$ and P is a sixth-degree polynomial expansion. The choice of the degree of the polynomial results from a compromise between accuracy and smoothness. Indeed, a larger degree would improve the accuracy, but spurious oscillations between the *ab initio* points are likely to happen.

$$P(Q_1, Q_2, Q_3) = c_0 + c_1 Q_1 + c_2 Q_3 + c_3 Q_1^2 + c_4 S_{2a}^2 + c_5 Q_1 Q_3 + c_6 S_{2b}^2 + c_7 Q_1^3$$
$$+ c_8 Q_1 S_{2a}^2 + c_9 S_3^3 + c_{10} Q_1^2 Q_3 + c_{11} Q_1 S_{2b}^2 + c_{12} Q_3 S_{2a}^2 + c_{13} Q_1^4 + c_{14} Q_1^2 S_{2a}^2$$
$$+ c_{15} S_{2a}^4 + c_{16} Q_1 S_3^3 + c_{17} Q_1^3 Q_3 + c_{18} Q_1^2 S_{2b}^2 + c_{19} Q_1 Q_3 S_{2a}^2 + c_{20} Q_3 S_3^3 + c_{21} S_{2a}^2 S_{2b}^2$$
$$+ c_{22} Q_1^5 + c_{23} Q_1^3 S_{2a}^2 + c_{24} Q_1 S_{2a}^4 + c_{25} Q_1^2 S_3^3 + c_{26} S_{2a}^2 S_3^3 + c_{27} Q_1^4 Q_3 + c_{28} Q_1^3 S_{2b}^2$$
$$+ c_{29} Q_1^2 Q_3 S_{2a}^2 + c_{30} Q_1 Q_3 S_3^3 + c_{31} Q_1 S_{2a}^2 S_{2b}^2 + c_{32} Q_3 S_{2a}^4 + c_{33} S_{2b}^2 S_3^3 + c_{34} Q_1^6$$
$$+ c_{35} Q_1^4 S_{2a}^2 + c_{36} Q_1^2 S_{2a}^4 + c_{37} Q_1^3 S_3^3 + c_{38} Q_1 S_{2a}^2 S_3^3 + c_{39} S_{2a}^6 + c_{40} S_3^6 + c_{41} Q_1^5 Q_3$$
$$+ c_{42} Q_1^4 S_{2b}^2 + c_{43} Q_1^3 Q_3 S_{2a}^2 + c_{44} Q_1^2 Q_3 S_3^3 + c_{45} Q_1^2 S_{2a}^2 S_{2b}^2 + c_{46} Q_1 Q_3 S_{2a}^4$$
$$+ c_{47} Q_1 S_{2b}^2 S_3^3 + c_{48} Q_3 S_{2a}^2 S_3^3 + c_{49} S_{2a}^4 S_{2b}^2, \qquad (7)$$

$$S_{2a}^2 = Q_2^2 + Q_3^2, \qquad (7a)$$

$$S_{2b}^2 = Q_2^2 - Q_3^2, \qquad (7b)$$

$$S_3^3 = Q_3^3 - 3Q_2^2 Q_3, \qquad (7c)$$

and Q_i ($i = 1,2,3$) are the D_{3h} symmetry coordinates defined by

$$\begin{bmatrix} Q_1 \\ Q_2 \\ Q_3 \end{bmatrix} = \begin{bmatrix} 1/\sqrt{3} & 1/\sqrt{3} & 1/\sqrt{3} \\ 0 & 1/\sqrt{2} & -1/\sqrt{2} \\ 2/\sqrt{6} & -1/\sqrt{6} & -1/\sqrt{6} \end{bmatrix} \begin{bmatrix} R_1 - 1 \\ R_2 - 1 \\ R_3 - 1 \end{bmatrix}. \qquad (8)$$

These coordinates can be used for an AB_2-type molecule, as long as R_2 and R_3 are chosen to label the two AB bond lengths.

Let us define now the functional form for the long-range potential energy (V_{LR})

$$V_{LR}(R_1, R_2, R_3) = \sum_{i=1}^{3} \left[f_i(R_1, R_2, R_3) \right.$$
$$\left. \times \sum_{n=n_i^{min}}^{n_i^{max}} U_{in}(\rho_i, \varphi_i) \chi_{in}(\rho_i) \right], \qquad (9)$$

where the sum on i runs over the three dissociation channels $H_a + OH_b^+$, $H_b + OH_a^+$, and $O + H_2^+$. The sum on n runs over the various contributions to the long-range interaction energy, which are defined below. For each dissociation channel ρ_i denotes the distance between the atom and the center of mass of the diatomic and φ_i the corresponding Jacobi angle (Figure 2). The function f_i is a switching function which selects the channel i.

$$f_i(R_1, R_2, R_3) = \frac{1}{2}\{1 - \tanh(\varsigma(3\delta_i - \delta_j - \delta_k))\}, \qquad (10)$$

with i $\neq$ j $\neq$ k, $\varsigma = 1$ bohr^{-1} and $\delta_i = R_i - R_i^e$, where R_i^e is the equilibrium distance of the diatomic molecule for the ith channel. Each dissociation channel is characterized by one internuclear distance close to the equilibrium value while the two other internuclear distances are large. The switching function f_i equals 1 in channel i because δ_i is small and δ_j and δ_k are both large, and it equals 0 in the two other channels because δ_i is large. For example, for $O + H_2^+$ (i. e., δ_2, $\delta_3 \rightarrow \infty$), f_1 is equal to 1 and f_2 and f_3 are equal to zero.

χ_{in} is a short-range damping function defined by

$$\chi_{in} = \left[1 - \exp\left(-\alpha\rho_i^2\right)\right]^n, \qquad (11)$$

with $\alpha = 0.2$ bohr^{-2} whatever i and n.

In the case of both $H_a + OH_b^+$ and $H_b + OH_a^+$ channels, we have a long-range interaction between an atom and a charged diatomic with a permanent dipole moment. The interaction energy can be written as a sum of three contributions

$$U_{i4}(\rho_i) = -\frac{e^2 \alpha_H}{2\rho_i^4 (4\pi\varepsilon_0)^2}, \qquad (12)$$

$$U_{i5}(\rho_i, \varphi_i) = -\frac{2e\alpha_H \mu_{OH^+} \cos(\varphi_i)}{\rho_i^5 (4\pi\varepsilon_0)^2}, \qquad (13)$$

$$U_{i6}(\rho_i, \varphi_i) = -\frac{\alpha_H \mu_{OH^+}^2 [3\cos^2(\varphi_i) + 1]}{2\rho_i^6 (4\pi\varepsilon_0)^2}, \qquad (14)$$

where i runs over 2 and 3.

With the arrangement $O + H_2^+$, we have a long-range interaction between an atom and a charged diatomic with no permanent dipole moment. Then, the interaction energy can be reduced to a single contribution

$$U_{14}(\rho_1) = -\frac{e^2 \alpha_O}{2\rho_1^4 (4\pi\varepsilon_0)^2}. \qquad (15)$$

The fitting procedure involves the determination of linear and nonlinear parameters. We used the following strategy: First, the nonlinear parameters ς and α were determined by the trial and error method. Then we used an iterative procedure for the other parameters. We choose a guess for the γ_i and R_i^0 nonlinear parameters and calculated the linear parameter with the weighted linear least squares. This step was repeated as necessary until the smallest possible RMS of the fitting error was reached. The fortran 90 subroutine of the PES is available upon request.

IV. VALIDATION OF THE 3D PES

The 25 515 MRCI BSSE corrected total energies were included in the global fit. The root mean square of the fit was less than 0.07 eV. Table I lists the numerical values of the parameters (c_j). We used $\alpha_O = 0.802$ Å^3 and $\alpha_H = 0.666793$ Å^3 and $\mu_{OH^+} = 1.00679$ debye for the definition of the long range parts of our 3D global PES. The α_I's are taken from Ref. 57 and μ_{OH^+} was computed at the MRCI level.

We display in Figure 3 the bi-dimensional cuts of this PES along the OH distances for bent structures (bending angle = 109°) and by varying one OH distance and the bending angle where the remaining OH distance is kept fixed at its equilibrium value (= 1.89 bohrs).

Figure 4 shows the one-dimensional cuts of the global 3D PES through the OH distance and by bending the molecule. The remaining coordinates are fixed to their values at equilibrium. We display also the MRCI energies (dots) for comparison. Close examination of this figure shows that the analytical fit reproduces quite well the *ab initio* energies along the OH distances for short and long ranges. Along the bending, the minimum is well fitted whereas one can see some deviations between the computed and fitted energies for bending angles in the 150°–170° range. This is, however, not significant. It should affect only slightly the quality of our analytical PES. In the following, we will compare the energetics, the spectroscopy of $H_2O^+(\tilde{X}^2B_1)$ and the long range behavior of our PES to the available data in the literature for validation.

A. Energetics and equilibrium geometry

For $H_2O^+(\tilde{X}^2B_1)$, we deduced from our 3D global PES the equilibrium geometry, the spectroscopic parameters, the
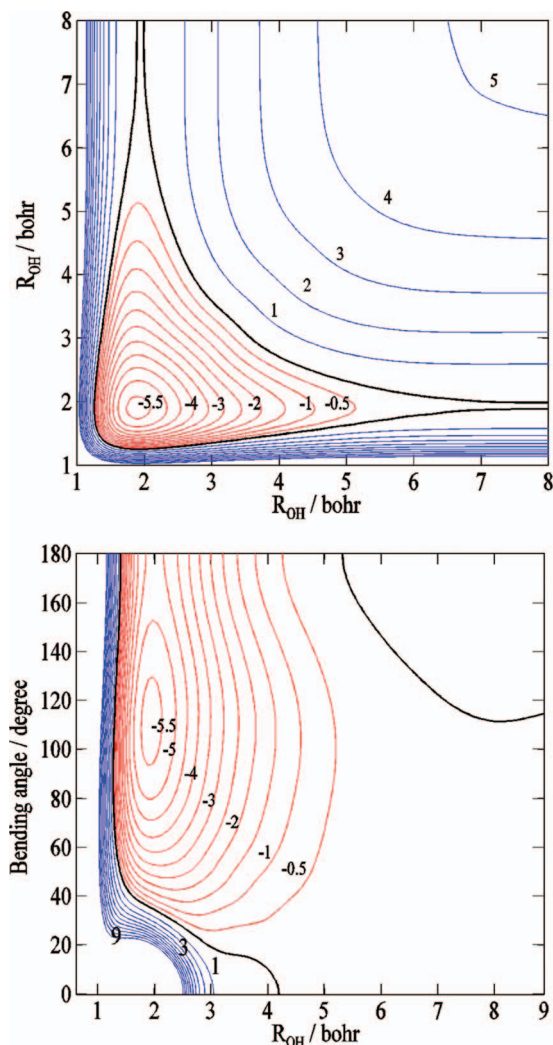
FIG. 3. Contour plots of our 3D-PES along the OH distances (top, bending angle = 109°) and along one OH distance and bending angle (bottom, R_{OH} = 1.89 bohrs). The zero of energy (black curve) is taken at the $OH^+(X^3\Sigma^-)$ + $H(^2S)$ dissociation. The steps between the contours are of 0.5 eV for the red ones and of 1 eV for the blue ones.
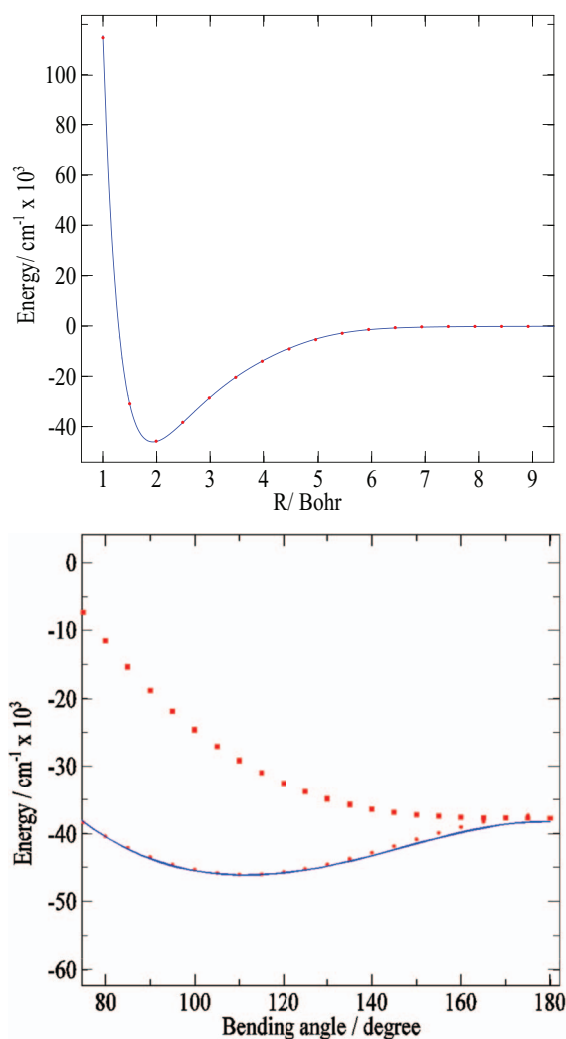

FIG. 4. Top: One-dimensional cut (solid line) of the global 3D-PES along the OH distance (R) where the other OH distance and in-plane bending angle are kept fixed to R_{OH} = 1.9 bohrs and 109°. Bottom: One-dimensional cut (solid line) of the global 3D-PES along the bending angle where both OH distances are kept fixed to R_{OH} = 1.89 bohrs. Dots are for the MRCI points of $H_2O^+(\tilde{X}^2B_1)$ and squares are for those of $H_2O^+(\tilde{A}^2A_1)$.

barrier to linearity, and the dissociation energy (D_e) for the formation of the $OH^+(X^3\Sigma^-)$ and $H(^2S)$ fragments. The results are given in Table II, where we list also previous theoretical and experimental data for comparison. Generally, a good agreement is observed. Indeed, we compute a OH distance of 0.999 Å, which coincides with the experimental values of Refs. 32 and 63. Our bending angle (of 109.7°) falls in between Lew's and Huet *et al.*'s determinations. Our OH distance is longer by 0.011 Å than that of Rosmus and co-workers[26] most likely because we use a larger basis set. Close agreement is also found for the rotational constants. The barrier to linearity is computed 1.095 eV, which is close to the measured one by Huet *et al.* (of 1.0209 eV).[32] Similarly, the present D_e matches those previously computed and measured ones.

B. Molecular region: Calculations of the spin ro-vibronic eigenstates of $H_2O^+(\tilde{X}^2B_1)$

The ground state of H_2O^+ ($\tilde{X}^2B_1$) correlates to a $^2\Pi_u$ state at linearity together with the H_2O^+ ($\tilde{A}^2A_1$) state

(Figure 4). Both components are coupled by the Renner-Teller effect (of linear-bent type) and by spin-orbit interaction. For sake of accuracy, we generated the 3D-PESs of these two components to be incorporated later in full variational treatment of the nuclear motions following the procedure described by Rosmus and co-workers.[26] Within this approach, the full dimensionality, anharmonicity, rotation-vibration, electronic angular momenta, and spin-orbit coupling effects are considered. Nevertheless, this variational procedure does not allow considering the global 3D-PES and the kinetic energy operator is implemented in internal coordinates. These internal coordinates correspond to the OH distances (r_1, r_2) and the in-plane bending angle (β) (Figure 2). Hence, we generated a 3D PES for $H_2O^+(\tilde{X}^2B_1)$ around the equilibrium minimum where $1.29 \leq r_{1,2} \leq 2.49$ bohrs, and $90° \leq \beta \leq 150°$. The energies were deduced from the analytical form of our 3D PES for 50 nonequivalent different geometries. For the $\tilde{A}$ state, we computed the energies at the MRCI/aug-cc-pV5Z for a grid of points composed by 30

TABLE II. Equilibrium geometry and spectroscopic characteristics for $H_2O^+(\tilde{X}^2B_1)$ deduced from our global 3D-PES.

	R_{OH} (Å)	HOH (deg)	A_e (cm^{-1})	B_e (cm^{-1})	C_e (cm^{-1})	ω_1 (cm^{-1})	ω_2 (cm^{-1})	ω_3 (cm^{-1})	Barrier to linearity (eV)	D_e (eV)
This work	0.999615	109.7	27.7040	12.6070	8.6643	3370.36	1479.28	3411.17	1.095	5.675
										5.895[a]
Theoretical works	0.98840[b]	109.30[b]								
		107.8[c]								
			27.9561[d]	12.5971[d]	8.6841[d]	3380.6[d]	1476.6[d]	3436.3[d]	0.9854[d]	
										5.7[e]
Exp. works	0.9988[f]	110.46[f]					1431.173[f]			
	0.9992[g]	109.30[g]							1.0209[g]	
			27.7040[h]	12.604[h]	8.6643[h]	3216[h]	1390.0[h]	3456.0[h]		
						3270[i]	1433.7[i]			

[a]Reference 58.
[b]Reference 26.
[c]Reference 59.
[d]Reference 60.
[e]Reference 61.
[f]Reference 62.
[g]Reference 32.
[h]Reference 63.
[i]Reference 64.

non-equivalent geometries around the $\tilde{A}$ state minimum (i.e., for $1.69 \leq r_{1,2} \leq 2.39$ bohrs, and $150° \leq \beta \leq 180°$). This allows covering the energy ranges up to $\sim 10\,000$ cm^{-1} above each minimum. Then, these total energies were fitted to the following polynomial expansions in displacement coordinates for both stretches and for the bending:

$$V(r_1, r_2, \beta) = \Sigma_{ijk} c_{ijk} Q_1{}^i Q_2{}^j Q_3{}^k, \quad (16)$$

with $Q_u = (r_u - r_u{}^{ref})$ for $u = 1$ and 2, and $Q_u = \beta - \beta^{ref}$ for $u = 3$ $(0° \leq \beta \leq 180°)$. The index "ref" refers to the reference geometry used in the fit, which is taken to be the equilibrium geometry of the considered electronic state. For $H_2O^+(\tilde{X}^2B_1)$, we used as reference $r_{1,2} = 1.893$ bohrs and $\beta = 109.7°$. For $H_2O^+(\tilde{A}^2A_1)$, we used the following reference geometry: $r_{1,2} = 1.868$ Å and $\beta = 180°$. A least squares procedure is used for fitting, where the root mean square of the fits is less than 1 cm^{-1}. Both 3D-PESs are strictly degenerate at linearity.

The resulting 3D-PES polynomial expansion coefficients are given as supplementary material (cf. Tables S1 and S2 of Ref. 65). They are used later to solve the nuclear motion problem using both standard second order perturbation theory[66,67] and the variational approach of Carter *et al.*[68,69] Perturbation theory allows deducing some spectroscopic parameters, which are given in Table S3.[65] The harmonic frequencies deduced from our PES are close to the *ab initio* values of Rosmus and co-workers,[60] whereas slight deviations can be seen with the experimental ones.[32,62–64] This is due to the difficulty to derive such quantities from the corresponding experimental spectra because of the complex vibronic structure of water cation where Renner-Teller and spin-orbit effects lead to non-conventional vibronic level pattern.[26]

Presently, the Renner-Teller problem is solved for $J = 1/2$. In the Hamiltonian, the $A_{SO}.\mathbf{L}.\mathbf{S}$ term is replaced by $A_{SO}.\mathbf{L_z}\mathbf{S_z}$ as justified by Brommer *et al.*[26] For any further technical details, we refer to their work. Indeed these authors showed convergence of the spin-rovibronic energy levels of

H_2O^+ upon the basis set used and approximations (e.g., non-dependence of the angular momenta on the nuclear positions). We used also their spin-orbit constant, A_{SO} ($= -130$ cm^{-1}).

The energies of the vibronic levels of H_2O^+, HDO^+, and D_2O^+ in their ground states are listed in Table III together with those calculated by Rosmus and co-workers[26] and those measured using photoelectron spectroscopy and threshold photoelectron spectroscopy.[38–40,64,70–72]

For H_2O^+, the symmetric stretch (ν_1) and the bending (ν_2) anharmonic frequencies are in excellent agreement with previous values since the differences fall within the error bars of these determinations. For instance, the ν_1 is computed here 3214.21 cm^{-1} and it was determined 3215.87 cm^{-1} by Rosmus and co-workers[26] and measured 3213.00 cm^{-1} using the highly resolved spectra by Jungen *et al.*[70] The bending anharmonic frequency (of 1414.09 cm^{-1}) is also close to their values (1412.15 and 1408.40 in cm^{-1}, respectively). The antisymmetric stretch (ν_3) shows slight deviations of ~ 13–15 cm^{-1} from theirs, which is acceptable given the small number of parameters (50) used to deduce the analytical global PES. The overtones and the combination modes of both modes deviate by less than 15 cm^{-1} from previous theoretical and experimental measurements attesting hence on the good description of our PES along the corresponding normal coordinates far from equilibrium. Similar remarks can be drawn when one compares the vibronic spectra for D_2O^+ and HDO^+ and the corresponding previously calculated and measured ones (see Table III for more details).

C. Long range and asymptotic behavior

For large internuclear separations, the PES should describe correctly the $OH^+(X^3\Sigma^-)$ and $H_2^+(X^2\Sigma_g^+)$ diatomics and the atom-diatom long range interaction. Table IV presents the spectroscopic constants deduced from a quantum calculation of the vibrational motion[74] using the two-body potential energy functions defined in Sec. III. These parameters include the equilibrium distances (r_e), the harmonic frequency (ω_e),

TABLE III. Variationally computed energies (in cm^{-1}) of the vibronic states of H$_2$O$^+$, HDO$^+$ and D$_2$O$^+$ in their ground electronic states deduced from the polynomial expansion (Eq. (16)).The rotationless levels (0_{00}) are listed.

Level	Calc.		Expt.				
(n_1, n_2, n_3)	MRCI This work	MRCI[a]	High resolution[b]	Low resolution[c]	Low resolution[d]	Low resolution[e]	Low resolution[f]
			H$_2$O$^+$				
(0,1,0)	1414.09	1412.15	1408.40	1407	1435.69	1427.61	1395.35
(0,2,0)	2782.61	2777.97	2771.27	2775	2814.90		2710.05
(1,0,0)	3214.21	3215.87	3213.00	3205	3266.58	3242.38	3202.05
(0,0,1)	3246.12	3261.80	3259.03				
(0,3,0)	4098.30	4092.32		4085	4250.58		4008.61
(1,1,0)	4607.19	4604.56		4593	4694.19	4645.82	4573.21
(0,1,1)	4635.62						
(0,4,0)	5346.68				5694.19		
(1,2,0)	5954.73	5947.92		5936	6097.61		5887.90
(0,2,1)	5982.46						
(2,0,0)	6289.39	6289.33		6280	6323.45	6396.04	6307.32
(0,0,2)	6297.20						
(1,0,1)	6465.19						
(0,5,0)	6495.52				6928.37		
(1,3,0)	7249.30	7241.26		7234	7589.75		
(0,3,1)	7281.07						
(0,6,0)	7520.69						
(2,1,0)	7657.11	7667.33		7639	7960.77	7767.20	7605.88
(0,1,2)	7663.33						
(1,1,1)	7832.40						
			D$_2$O$^+$				
(0,1,0)	1049.21	1047.43	1044.27	1045	1072.72	1064.67	1056.61
(0,2,0)	2074.87	2070.14		2063	2088.99		
(1,0,0)	2348.47	2350.71		2342	2371.29	2363.25	2347.12
(0,0,1)	2416.34						
(0,3,0)	3075.15	3066.45	3058.66	3007	3202.05		
(1,1,0)	3386.95	3385.94		3373	3403.69	3395.67	3355.34
(0,1,1)	3452.61						
(0,4,0)	4047.15				4113.47		
(1,2,0)	4401.29	4396.26		4396	4428.03		
(0,2,1)	4466.33						
(2,0,0)	4644.89	4648.17		4638	4645.80	4661.99	
(0,0,2)	4684.28						
(1,0,1)	4799.10						
(0,5,0)	4986.13				5024.94		
(1,3,0)	5390.04				5484.69		
(0,3,1)	5456.12						
(2,1,0)	5672.11	5670.92		5650	5960.57	4621.66	5662.14
(0,1,2)	5709.21						
(1,1,1)	5822.46						
(2,2,0)	6674.40	6668.64		6694			
(3,0,0)	6867.30	6880.38		6860	6855.87	6920.39	
			HDO$^+$				
(0,1,0)	1246.68	1244.62					
(1,0,0)	2380.43	2387.93					
(0,2,0)	2460.93						
(0,0,1)	3228.93	3238.42					
(1,1,0)	3605.38	3606.06					
(0,3,0)	3645.84						
(0,1,1)	4450.45	4456.10					
(2,0,0)	4679.59	4691.72					
(0,4,0)	4753.25						
(1,2,0)	4831.02	4828.14					
(1,0,1)	5605.02	5618.87					
(0,2,1)	5643.07	5645.45					

TABLE III. (*Continued.*)

	HDO$^+$						
Level	Calc.		Expt.				
(n_1,n_2,n_3)	MRCI This work	MRCI[a]	High resolution[b]	Low resolution[c]	Low resolution[d]	Low resolution[e]	Low resolution[f]
(0,5,0)	5825.24						
(2,1,0)	5899.78						
(1,3,0)	5998.44	5907.79					
(0,0,2)	6293.87	6317.37					
(0,3,1)	6772.89						
(0,6,0)	6810.11						
(1,1,1)	6831.45						
(3,0,0)	6888.82						

[a]Reference 26.
[b]References 70–72.
[c]Reference 64.
[d]Reference 38.
[e]Reference 39.
[f]Reference 40.
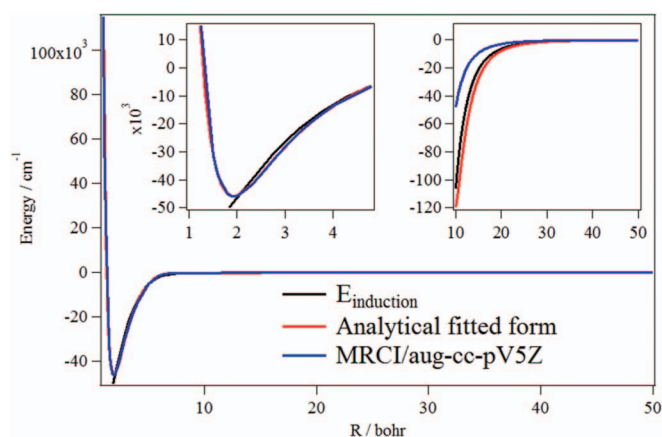
FIG. 5. Behavior of energy for long range arrangement H + OH$^+$ (bending angle HOH = 110° and OH distance = 1.9 bohrs). Blue curve: MRCI/aug-cc-pV5Z computed energies. Red curve: Analytical form. Black curve: $E_{induction}$ corresponds to the induction contribution, whereas the electrostatic and dispersion terms are negligible.

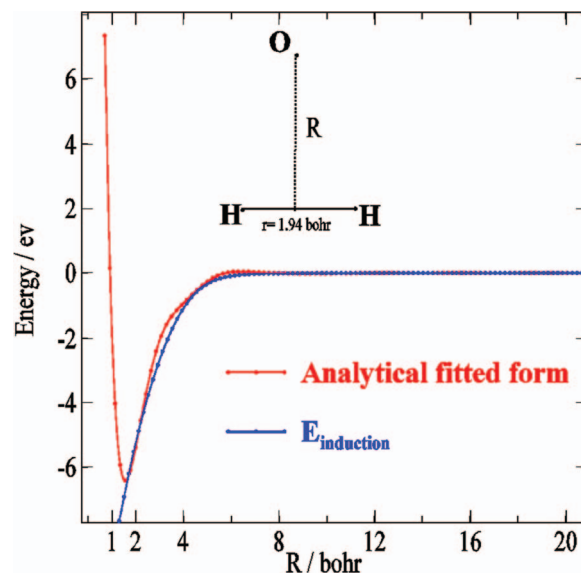FIG. 6. Behavior of the interaction energy for long range arrangement O + H$_2^+$ in C$_{2v}$ symmetry. Blue curve: analytical form. Red curve: $E_{induction}$.

TABLE IV. Spectroscopic constants for OH$^+$(X$^3\Sigma^-$) and H$_2^+$(X$^2\Sigma_g^+$). First entry: experimental values from Ref. 73. Second entry: this work. See text for more details.

	r_e (Å)	ω_e (cm^{-1})	$\omega_e x_e$ (cm^{-1})	D_e (eV)
H$_2^+$(X$^2\Sigma_g^+$)	1.052	2321.7	66.2	2.7925
	1.056	2318.64	63.58	2.7925
OH$^+$(X$^3\Sigma^-$)	1.0289	3113.37	78.52	5.300
	1.0285	3115.29	78.24	5.166

the anharmonic term ($\omega_e x_e$), and the dissociation energy (D$_e$). For both diatomics, the deviations between our values and the experimental ones[73] are ~2%–4%. This represents a satisfactory agreement.

We present in Figure 5 the long range behavior of the PES for the H + OH$^+$ arrangement. This figure compares the PES with the MRCI energy and with the induction interaction as calculated with Eqs. (12)–(14). A good overall agreement is shown. However, the induction interaction and the fitted PES are slightly more attractive than the MRCI energies for R < 20 bohrs. In order to illustrate the long range behavior of the arrangement O + H$_2^+$, we compared the fitted PES with the long-range induction interaction (Eq. (15)). A good agreement is found (Figure 6).

V. CONCLUSIONS AND PERSPECTIVES

We generated the BSSE corrected global 3D-PES of $H_2O^+(\tilde{X}^2B_1)$ ground state. The electronic computations were performed at the MRCI/aug-cc-pV5Z. An analytic form is deduced that covers both molecular and long ranges. For validation, we compared the spectroscopic constants of $H_2O^+(\tilde{X}^2B_1)$ and of its fragments, and the vibronic spectrum of $H_2O^+(\tilde{X}^2B_1)$ to the available experimental and theoretical data. A good agreement is found.
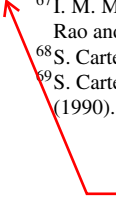
Form a perspective point of view, this PES will be used to compute the rotation-vibration spectrum of "hot water cation." For instance, this is of great importance for the chemistry and for the detection of this cation in Sun. Briefly, this goes through the deduction of the H_2O^+ transitions after incorporation of our 3D-PES and the 3D dipole moment surface of $H_2O^+(\tilde{X}^2B_1)$.[75] In related topic, Polyansky and co-workers proved the existence of neutral water on Sun after accurate computations of the rotation-vibration transitions for water that coincide with sun lines.[76,77] Moreover, we are planning to explore the fragmentation dynamics of H_2O^+ to form the $H + OH^+$ products and its isotopolog variants as widely done for the neutral water in Refs. 17–22.

[1] L. Che, Z. Ren, X. Wang, W. Dong, D. Dai, X. Wang, D. H. Zhang, X. Yang, L. Sheng, G. Li, H.-J. Werner, F. Lique, and M. H. Alexander, Science **317**, 1061 (2007).

[2] M. Qiu, Z. Ren, L. Che, D. Dai, S. A. Harich, X. Wang, X. Yang, C. Xu, D. Xie, M. Gustafsson, R. T. Skodje, Z. Sun, and D. H. Zhang, Science **311**, 1440 (2006).

[3] M. Tizniti, S. D. Le Picard, F. Lique, C. Berteloite, A. Canosa, M. H. Alexander, and I. R. Sims, Nat. Chem. **6**, 141 (2014).

[4] F. Lique, M. Jorfi, P. Honvault, P. Halvick, S. Y. Lin, H. Guo, D. Q. Xie, P. J. Dagdigian, J. Kłos, and M. H. Alexander, J. Chem. Phys. **131**, 221104 (2009).

[5] F. Lique, G. Werfelli, P. Halvick, T. Stoecklin, A. Faure, L. Wiesenfeld, and P. J. Dagdigian, J. Chem. Phys. **138**, 204314 (2013).

[6] B. Bussery-Honvault, F. Dayou, and A. Zanchet, J. Chem. Phys. **129**, 234302 (2008).

[7] A. Zanchet, B. Bussery-Honvault, and P. Honvault, J. Phys. Chem. A **110**, 12017 (2006).

[8] M. Pavanello, L. Adamowicz, A. Alijah, N. F. Zobov, I. I. Mizus, O. L. Polyansky, J. Tennyson, T. Szidarovszky, A. G. Császár, M. Berg, A. Petrignani, and A. Wolf, Phys. Rev. Lett. **108**, 023002 (2012).

[9] O. L. Polyansky, R. I. Ovsyannikov, A. A. Kyuberis, L. Lodi, J. Tennyson, and N. F. Zobov, J. Phys. Chem. A **117**, 9633 (2013).

[10] R. Dawes, P. Lolur, A. Li, B. Jiang, and H. Guo, J. Chem. Phys. **139**, 201103 (2013).

[11] See http://webbook.nist.gov for the dissociation energies of H_2O^+ cation and the excitation energies of the corresponding fragments.

[12] G. Herzberg, Ann. Geophys. **36**, 605 (1980).

[13] B. L. Lutz, M. Womak, and R. M. Wagner, Astrophys. J. **407**, 402 (1993).

[14] D. Smith, Chem. Rev. **92**, 1473 (1992).

[15] D. Hollenbach, M. J. Kaufman, D. Neufeld, M. Wolfire, and J. R. Goicoechea, Astrophys. J. **754**, 105 (2012).

[16] P. Schilke, D. C. Lis, E. A. Bergin, R. Higgins, and C. Comito, J. Phys. Chem. A **117**, 9766 (2013).

[17] R. Martínez, J. Millán, and M. González, J. Chem. Phys. **120**, 4705 (2004).

[18] R. Martínez, J. D. Sierra, and M. González, J. Chem. Phys. **123**, 174312 (2005).

[19] R. Martínez, J. M. Lucas, X. Giménez, A. Aguilar, and M. González, J. Chem. Phys. **124**, 144301 (2006).

[20] R. Martínez, J. D. Sierra, S. K. Gray, and M. González, J. Chem. Phys. **125**, 164305 (2006).

[21] W. Xu, W. Li, and P. Zhang, Comput. Theor. Chem. **1012**, 1 (2013).

[22] C. Jia-Wu, L. Xin-Guo, S. Hai-Zhu, and Z. Qing-Gang, Chin. Phys. Lett. **28**, 093101 (2011).

[23] A. G. Sage, T. A. A. Oliver, R. N. Dixon, and M. N. R. Ashfold, Mol. Phys. **108**, 945 (2010).

[24] A. J. Lorquet and J. C. Lorquet, Chem. Phys. **4**, 353 (1974).

[25] D. Deharang, X. Chapuisat, J. C. Lorquet, C. Galloy, and G. Raseev, J. Chem. Phys. **78**, 1246 (1983).

[26] M. Brommer, B. Weis, B. Follmeg, P. Rosmus, S. Carter, N. C. Handy, and P. J. Knowles, J. Chem. Phys. **98**, 5222 (1993).

[27] S. Wu, Y. Chen, X. Yang, Y. Guo, Y. Liu, Y. Li, R. J. Buenker, and P. Jensen, J. Mol. Spectrosc. **225**, 96 (2004).

[28] M. Eroms, M. Jungen, and H.-D. Meyer, J. Phys. Chem. A **114**, 9893 (2010).

[29] Y. Gan, X. Yang, Y. Guo, S. Wu, W. Li, Y. Liu, and Y. Chen, Mol. Phys. **102**, 611 (2004).

[30] S. Wu, X. Yang, Y. Guo, H. Zhuang, Y. Liu, and Y. Chen, J. Mol. Spectrosc. **219**, 258 (2003).

[31] T. R. Huet, I. H. Bachir, J.-L. Destombes, and M. Vervloet, J. Chem. Phys. **107**, 5645 (1997).

[32] T. R. Huet, C. J. Pursell, W. C. Ho, B. M. Dinelli, and T. Oka, J. Chem. Phys. **97**, 5977 (1992).

[33] P. R. Brown, P. B. Davies, and R. J. Stickland, J. Chem. Phys. **91**, 3384 (1989).

[34] H. Lew and I. Heiber, J. Chem. Phys. **58**, 1246 (1973).

[35] S. E. Strahan, R. P. Mueller, and R. J. Saykally, J. Chem. Phys. **85**, 1252 (1986).

[36] P. Mürtz, L. R. Zink, K. M. Evenson, and J. M. Brown, J. Chem. Phys. **109**, 9744 (1998).

[37] M. S. Forda, K. Müller-Dethlefs, M. Kitajima, H. Tanaka, Y. Tamenori, A. De Fanis, and K. Ueda, J. Phys. Chem. A **114**, 11133 (2010).

[38] S. Y. Truong, A. J. Yencha, A. M. Juarez, S. J. Cavanagh, P. Bolognesi, and G. C. King, Chem. Phys. **355**, 183 (2009).

[39] L. Karlsson, L. Mattsson, R. Jadrny, R. G. Albridge, S. Pinchas, T. Bergmark, and K. Siegbahn, J. Chem. Phys. **62**, 4745 (1975).

[40] R. N. Dixon, G. Duxbury, J. W. Rabalais, and L. Åsbrink, Mol. Phys. **31**, 423 (1976).

[41] H.-J. Werner, P. J. Knowles, G. Knizia, F. R. Manby, M. Schütz *et al.*, MOLPRO, version 2012.1, a package of *ab initio* programs, 2012, see http://www.molpro.net.

[42] P. J. Knowles and H.-J. Werner, Chem. Phys. Lett. **115**, 259 (1985).

[43] H.-J. Werner and P. J. Knowles, J. Chem. Phys. **82**, 5053 (1985).

[44] H.-J. Werner and P. J. Knowles, J. Chem. Phys. **89**, 5803 (1988).

[45] P. J. Knowles and H.-J. Werner, Chem. Phys. Lett. **145**, 514 (1988).

[46] T. H. Dunning, J. Chem. Phys. **90**, 1007 (1989).

[47] R. A. Kendall, T. H. Dunning, Jr., and R. J. Harrison, J. Chem. Phys. **96**, 6796 (1992).

[48] D. E. Woon and T. H. Dunning, Jr., J. Chem. Phys. **98**, 1358 (1993).

[49] D. E. Woon and T. H. Dunning, Jr., J. Chem. Phys. **103**, 4572 (1995).

[50] S. F. Boys and F. Bernardi, Mol. Phys. **19**, 553 (1970).

[51] T.-S. Ho and H. Rabitz, J. Chem. Phys. **104**, 2584 (1996).

[52] T. Hollebeek, T.-S. Ho, and H. Rabitz, Annu. Rev. Phys. Chem. **50**, 537 (1999).

[53] T. Stoecklin and Ph. Halvick, Phys. Chem. Chem. Phys. **7**, 2446 (2005).

[54] G. C. Maitland, M. Rigby, E. B. Smith, and W. A. Wakeham, *Intermolecular Forces; Their Origins and Determination* (Clarendon, Oxford, 1981).

[55] J. N. Murrell, K. S. Sorbie, and A. J. C. Varandas, Mol. Phys. **32**, 1359 (1976).

[56] A. J. C. Varandas, J. Brandao, and L. A. M. Quintales, J. Phys. Chem. **92**, 3732 (1988).

[57] M. Miller and B. Bederson, Adv. At. Mol. Phys. **13**, 1 (1977).

[58] H. Kayi, I. B. Bersukerand, and J. E. Boggs, J. Mol. Struct. **1023**, 108 (2012).

[59] R. A. Rose, S. J. Greaves, and A. J. Orr-Ewing, J. Chem. Phys. **132**, 244312 (2010).

[60]B. Weiss, S. Carter, P. Rosmus, P. J. Knowles, and H.-J. Werner, J. Chem. Phys. **91**, 2818 (1989).

[61]B. M. Hughesand and T. O. Tiernan, J. Chem. Phys. **55**, 3419 (1971).

[62]H. Lew, Can. J. Phys. **54**, 2028 (1976).

[63]B. M. Dinelli, M. W. Crofton, and T. Oka, J. Mol. Spectrosc. **127**, 1 (1988).

[64]J. E. Reutt, L. S. Wang, Y. T. Lee, and D. A. Shirley, J. Chem. Phys. **85**, 6928 (1986).

[65]See supplementary material at http://dx.doi.org/10.1063/1.4872329 for 3D PESs of ground and first excited electronic states of H_2O^+ and their spectroscopic terms.

[66]SURFIT, a program written by J. Senekowitsch, thesis of the University of Frankfurt, Germany, 1988.

[67]I. M. Mills in *Molecular Spectroscopy: Modern Research*, edited by K. N. Rao and C. W. Mathews (Academic Press, 1972).

[68]S. Carter and N. C. Handy, Mol. Phys. **52**, 1367 (1984).

[69]S. Carter, N. C. Handy, P. Rosmus, and G. Chambaud, Mol. Phys. **71**, 605 (1990).

[70]Ch. Jungen, K. E. Hallin, and A. J. Merer, Mol. Phys. **40**, 25 (1980).

[71]Ch. Jungen, K. E. Hallin, and A. J. Merer, Mol. Phys. **40**, 65 (1980).

[72]"The spectroscopy of molecular ions," in *Proceedings of a Royal Society Discussion Meeting*, organized and edited by A. Carrington and B. H. Thrush (The Royal Society, London, 1988).

[73]K. P. Huber and G. Herzberg, *Molecular Spectra and Molecular Structure, Constants of Diatomic Molecules* Vol. 4 (Van Nostrand Reinhold, New York, 1979).

[74]J. W. Cooley, Math. Comput. **15**, 363 (1961).

[75]M. A. Gannouni, N. E. Jaidane, P. Halvick, T. Stoecklin, and M. Hochlaf (unpublished).

[76]O. L. Polyansky, N. F. Zobov, S. Viti, J. Tennyson, P. F. Bernath, and L. Wallace, Science **277**, 346 (1997).

[77]O. L. Polyansky, A. G. Csaszar, S. V. Shirin, N. F. Zobov, P. Barletta, J. Tennyson, D. W. Schwenke, and P. J. Knowles, Science **299**, 539 (2003).

66~69